Part 1

NOVEL NANOSTRUCTURES AND DEVICES

© 2003 Zikang Tang and Ping Sheng/CRC Press LLC

1 Nanopatterning with Diblock Copolymers

P. M. Chaikin[1,2], C. Harrison[1], M. Park[1], R. A. Register[2,3], D. H. Adamson[2], D. A. Huse[1], M. A. Trawick[1], R. Li[4] and P. Dapkus[4]
[1]Department of Physics, [2]Princeton Materials Institute, [3]Department of Chemical Engineering, [4]Princeton University, Princeton, New Jersey 08544, Compound Semiconductor Laboratory, Department of Electrical Engineering/ Electrophysics, University of Southern California, Los Angeles, CA 90089

1.1 INTRODUCTION

There has been an interest in going beyond conventional lithographic techniques in order to make features of ever smaller scale and higher density over large areas. In this paper we discuss progress that has been made over the past decade in using the self-assembly of diblock copolymer films as a template for creating two dimensional patterns (lines and dots) with a characteristic spacing of 20-30 nm. Typically trillions of dots, holes, posts of semiconductors and metals are produced on conventional semiconductor wafers. We describe the basic concept of the pattern formation and the technology of the transfer of the pattern from soft to hard materials. In order to produce and study these nanoscopic patterns we had to develop some new techniques for getting two and three dimensional images. 3D depth profiling with reactive ion etch (RIE) slices of 7 nm thickness alternating with electron microscope pictures proved very effective. We became very interested in the pattern formation and annealing necessary to control the long range order of the arrays and found new ways to follow the ordering. The coarsening was found to obey a $t^{1/4}$ power law, (that is the size of the "grains" grew with time with this dependence) and at least for the striped pattern (cylinders lying down in a fingerprint like pattern) we could understand the microscopic origin of this behavior. We studied these phenomena with time lapse AFM microscopy and found that the disorder was dominated by the presence of disclinations and the annealing occurred by the annihilation of disclination multipoles rather than simple disclination – antidisclination, dipole dynamics. We also found that the orientation of the patterns could be controlled by introducing alignment marks, step edges.

© 2003 Zikang Tang and Ping Sheng/CRC Press LLC

1.1.1 Why Nanolithography?

Our interest in periodic patterns on the nanometer scale originated in a physics problem, the Hofstadter (1976) "butterfly", a problem of incommensurability between a periodic potential and flux quantization in a magnetic field. The competition of lengths-scales leads to a fascinating fractal energy spectrum. The best way to observe these effects is to take a quantum Hall device in the lowest Landau level and decorate it with a periodic potential on the scale of the cyclotron radius (Thouless, 1982). For a magnetic field of 1 Tesla the characteristic magnetic length, l, which gives a flux quanta (ϕ_0=hc/e) through its area ($Hl^2= \phi_0$) is l~20 nm. We therefore wanted to create a two dimensional lattice with unit cells on this scale and transfer a potential from this pattern to the two dimensional electron gas that resides about 20 nm below the surface of a quantum Hall device. Lithographic techniques are constantly evolving and the feature size is getting smaller. Presently large scale integrated devices (like Pentium chips) are produced by optical lithography with feature size >150 nm. Smaller features are readily produced by electron beam lithography, down to >25 nm, but it is difficult to place such features next to one another at the same scale and to produce periodic arrays of them. Moreover it is extremely time consuming to cover large areas with such patterns if each must be separately written, even once.

Aside from the Hofstadter spectrum such dense periodic arrays should have interest for magnetic disk drives, for addressable memories, as optical elements, for quantum dots, for excitation and transfer between dye molecules and in biology as filters and sensors for proteins and nucleic acid sections. In many of these applications, e.g. filters, disks drives, quantum dots, it is the size and density that are of interest, while in other applications the periodicity and long range order are required.

Our interest in using diblock copolymers for this work was initiated in discussions with Dr. Lew Fetters who had studied the synthesis and three dimensional structure of different diblock copolymer phases (Morton, 1975). The cross sections of his samples showed beautiful lattices with spacings on the 20 nm scale and perfect order over many microns. The idea of transferring these patterns to other organic and inorganic substrates was attractive since the copolymer self-assembly could be done over large scales simultaneously, the morphology and length scale were chemically modifiable and the materials were fairly easy to work with. The basic physical and chemical properties of the diblock copolymers were already a well developed science in the bulk and they could be readily processed by techniques used in conventional semiconducting lithography. The fact that nanoscale patterns remained suitable in thin films was demonstrated by Mansky et al. (Mansky, 1995, 1996).

© 2003 Zikang Tang and Ping Sheng/CRC Press LLC

1.1.2 Basics of Diblock Copolymers

Consider two types of monomers, A and B, which have a net repulsive interaction. When we make a polymer of each AAAAAAAA and BBBBBBB, the repulsive interaction between the segments is enhanced (by the number of monomers per segment) and a mixture of the two would phase separate like oil and water with one floating above the other (de Gennes, 1979). However, if the segments or blocks are covalently bound, AAAAAAAA BBBBBBB, making a diblock copolymer, figure 1a), they cannot macroscopically phase separate. The best that they can do is microphase separate putting all the A's together and all the B's together with an interface between them. If the blocks are of similar length then the arrangement shown in figure 1b) is appropriate and a lamellar phase results. If the A segment is much smaller than

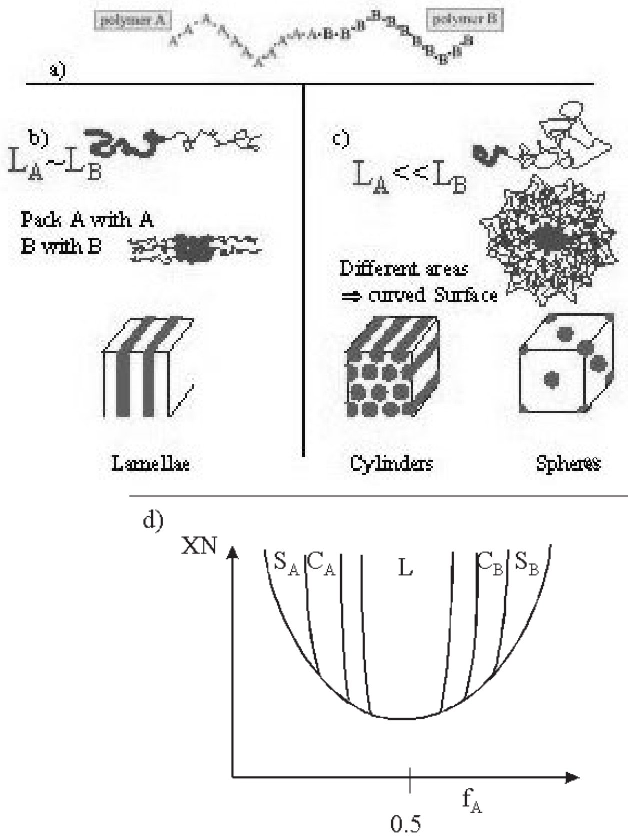

Figure 1 a) Schematic of diblock copolymer. b) Microphase separation into lamellae when A and B segments have about the same length. c) Cylindrical and Spherical phases form when segments have very different length. d) Mean field phase diagram of as a function of total repulsion between segments XN and fraction of diblock which is A monomers.

© 2003 Zikang Tang and Ping Sheng/CRC Press LLC

the B segment, figure 1c) then the area on the A side of the interface is smaller than on the B side and there is a natural curvature to the interface. The result is cylinders or spheres which arrange on a Hexagonal or Body Centered Cubic lattice respectively.

The mean field phase diagram as originally calculated by Leibler (1980) is shown schematically in figure 1d). • is the Flory parameter (Flory, 1953) which characterizes the repulsive interaction and N is the polymerization index (number of monomers per polymer) and for a specific monomer is proportional to the polymer molecular weight. •N is then a measure of the total repulsion between polymer blocks and the microphase separation occurs when that energy overcomes the mixing entropy. f_A is the fraction of diblock which is A. As suggested above we have lamellae when there are equal A and B length or $f_A = 0.5$. For A rich phases ($f_A > .5$) we have regions of B in a continuous matrix of A and conversely for B rich phases ($f_A < .5$). The actual phase diagram depends on the actual intermolecular interactions and asymmetries and is considerably more complex with fascinating multiple interconnected phases such as the gyroid. Interested readers are referred to the excellent reviews by Bates (Bates, 1990, Bates, 1991). For our purposes the cylindrical and spherical phases are most useful.

Figure 2 Cartoon of monolayer films of spherical and cylindrical phase diblock copolymers with rubber component wetting both surfaces.

From what we know of the three dimensional phase diagram we thought that we could make monolayers, as cartooned in figure 2 which we might use to pattern transfer and form lines or dots in inorganic materials. What controls the length scale? Clearly the stretched length of the polymer, **Na**, where **a** is a monomer size, is a limit. The actual scaling is a playoff between the interfacial energy, σ, between the A and B rich phases, and the elastic energy in stretching the polymers. Consider a particular structure, say spheres, which is set by f_A the ratio of A to B. We want to know the size of a microphase separated region, a micelle, and the number of polymers, n, associated with it. If the length scale is R then the interfacial energy is the area S times the surface tension, σ, or $S\sigma/n$ ($=4\pi R^2\sigma/n$) per polymer. The number of monomers in the micelle is proportional to the number of polymers times the number of monomers per polymer chain, nN. It is also proportional to the volume V of the micelle times the monomer density ρ, or $n = \rho V/N$. If the chains are Gaussian and are stretched to a length R then the harmonic elastic energy per chain is $(3/2)(R^2/Na^2)k_BT$. The Elastic plus interfacial energy is $S\sigma N/\rho V + (3/2)(R^2/Na^2)k_BT = C(\sigma N/\rho R) + (3/2)(R^2/Na^2)k_BT$, where $C = SR/V = 3$ for spheres, 2 for cylinders and 1 for lamellae. Minimizing with respect to R we have $R = N^{2/3}(C\sigma a^2/3\rho k_BT)^{1/2}$.

© 2003 Zikang Tang and Ping Sheng/CRC Press LLC

$$R = N^{\frac{2}{3}}\left(\frac{\left(C\sigma a^2\right)}{3\rho k_B T}\right) \quad (1.1)$$

Typically for a Polystyrene-Polybutadiene, PS-PB, diblock with molecular weight PS-PB 65-10 kg/mol we have PB spheres of 10 nm diameter with a center to center spacing of 25 nm. The spherical micelles consist of about 100 PB chains with about 100 monomers per chain. The size and periodicity will scale with molecular weight to the 2/3 power.

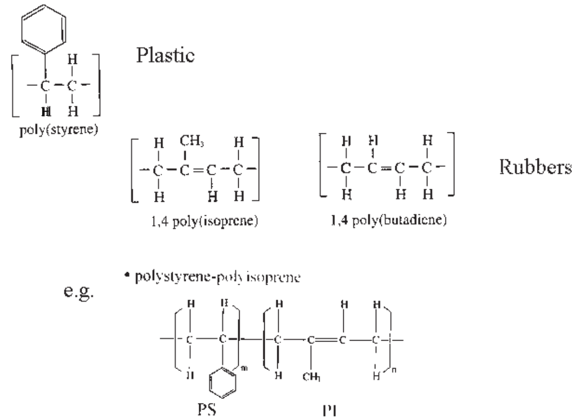

Figure 3 The diblocks we use are usually a plastic and a rubber as in the monomers and diblock shown here.

The polymers that we used were generally a plastic (such as polystyrene) and a rubber (such as polybutadiene or polyisoprene, PI), figure 3. For observation and pattern transfer we need some contrast between the two parts of the diblock. What proved convenient for many of our studies and for processing was to use the fact that the PB backbone had a double bond, while the PS did not. Reactions with the double bond were used both to stain and crosslink the PB and PI with Osmium tetroxide for SIMS and electron microscopy and to break the double bond and fragment the PI and PB by ozonation for processing. For AFM imaging the contrast was supplied by the different elastic properties (stiffness) of the rubbers and plastics.

1.2 IMAGING AND DEPTH PROFILING

The basic idea of using a diblock copolymer for patterning a substrate is straightforward, put down a monolayer, use some contrast between the blocks as a mask and then etch through to the substrate (Harrison, 1998). However, each step required extensive new investigations not the least of which was figuring out what we had before the transfer took place.

© 2003 Zikang Tang and Ping Sheng/CRC Press LLC

1.2.1 Sample Preparation

The diblocks we used were soluble in toluene and a conventional spin coater was used to cast a film on commercial Si wafers. The polymer concentration, volume and spin rate determine the thickness. Thickness measurements were accomplished largely by ellipsometry, interferometry and secondary ion mass spectrometry (SIMS). It is well known that ordered diblock films are quantized in thickness due to the discreet layer spacing (Coulon, 1990, Mansky, 1995b). If you spin coat a copolymer film at a thickness equal on average to 1.5 layers after annealing, the result is half the surface coated with a monolayer and the other half with two monolayers, usually in islands. For such thin films the layer thicknesses do not correspond to the bulk layer thickness since one or the other polymer preferentially wets the substrate and the air which bound the film. The cartoons which are shown in figure 2 are what we deduced from many experiments and then confirmed by performing SIMS with OsO_4 staining of the rubber component (Harrison, 1998). There have been several studies of the effects of surface treatment on which polymer wets the surface and the different morphologies which result (Ahagon, 1975, Jones, 1992, Hashimoto, 1992). With neutral surfaces both phases can wet and the result is cylindrical films (and lamellar films) which form perpendicular to the surface rather than lie flat (Huang, 1998, 2000, Harrison, 2000). A good bit of work went into understanding how the morphology of the films depend on their thickness (Henke, 1988, Anastasiadis, 1989, Mansky, 1995a, Park, 1997b, Radzilowski, 1996). For example, if we start with a sample with cylinders of PB in a PS matrix, a bulk layer spacing of 30 nm and PB wets the surface then: a 30 nm thickness film will not even phase separate, a 40 nm film will have a layer of PB spheres, and a 50 nm layer will have the desired cylindrical morphology cartooned in figure 2. The hand waving explanation is that the surface layers rob PB from the phase separated interior region and effectively reduce f_A in the phase diagram of figure 1d).

1.2.2 3D Imaging

In our original studies of monolayer films we used TEM images made through a SiN window prepared on a Si wafer (Morkved, 1994, 1996, Park, 1997). This allowed us a projection view of the pattern over a region about 10 micron square. In order to further develop the science and technology necessary for this process we needed to observe the pattern over larger scale and on the actual surface that we hoped to decorate. The answer was to take SEM images of the monolayer with contrast supplied by the OsO_4 staining. Unfortunately, the wetting layers on these films were the rubbery component, which was the stained phase. SEM revealed only the uniform surface and none of the interior structure we were after. The surface had to be removed. The answer was to reactive ion etch to a depth where the microphase separated regions could be observed. A number of different gases and procedures were tried (Harrison, 1999). Some of our observation include: Ar gives a very rough etch of both PS and PB, Cl_2 destroys the microstruture, $ClHF_3$ and O_2 give a rough etches of PB and PS, CF_4 gives smooth etches on PS, PB and PB with OsO_4 stain. The choice was the CF_4 at a rate of about 20 nm/minute. The etch was sufficiently smooth and nonpreferential that we could step through the

© 2003 Zikang Tang and Ping Sheng/CRC Press LLC

monolayer and see the surface, the bulk continuous phase, the micelles etc. We would remove a slice, take a SEM image, remove another slice, take another image etc. What was particularly surprising was that the etch did not seem to produce additional roughness even for thick samples (Harrison, 1998a). With ten –twenty layers we could image the last layer with essentially the same flatness and resolution as the first (Harrison, 1998b). With experiments on trilayer islands, figure 4, it was possible to follow the structures and defects through three layers, to see that the patterns were interdigitated and to establish the depth resolution as ~7 nm (Harrison, 1997). This technique therefore allows three dimensional real space imaging of many soft materials and has been exploited by several groups. For example between successive RIE slice removal the imaging step can be done by AFM instead of SEM.

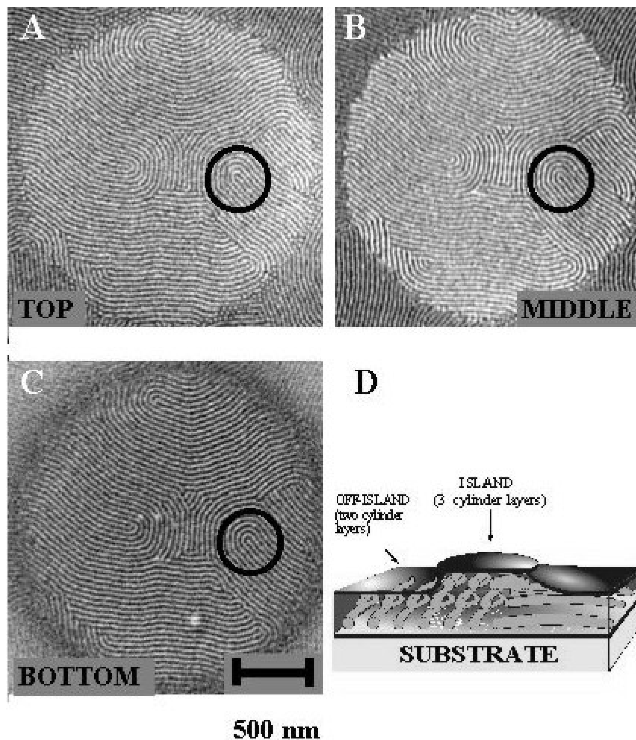

Figure 4 SEM images of a three layer island after RIE removal to reveal structures at different depths. Note the alternate white-black lines in the circle indicating interdigitation of disclination pattern.

1.3 PATTERN TRANSFER TECHNIQUES

Having established that we could form monolayers of the appropriate hexagonal dots or parallel lines on a surface the next challenge was finding a way to transfer the patterns to a substrate. The obvious technique was RIE, but again the

© 2003 Zikang Tang and Ping Sheng/CRC Press LLC

questions involved what gases would recognize the polymer as a mask and what to use for the contrast in the diblock pattern.

1.3.1 Basic Positive and Negative Techniques

CF_4 was an ideal gas for uniformly etching PS and PB at essentially the same rate. It also provided a reasonable but rougher etch into Si and SiNx. Directly

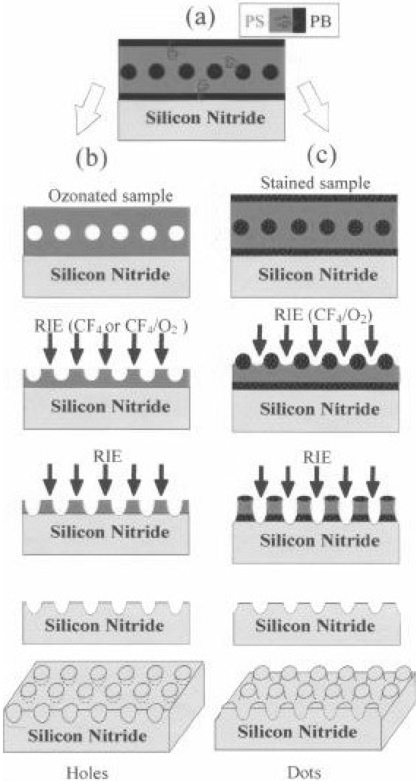

Figure 5 Process flow chart for transferring positive or negative patterns from diblock monolayer to etched features in substrate.

etching with CF_4 would therefore provide no contrast or pattern transfer. The answer was to remove one of the components of the diblock and this was accomplished by again taking advantage of the double bonds in the rubbery phase. Ozone attacks these double bonds and leaves small polymer segments which are volatile and soluble. The easiest processing step to degrade the PB is to immerse the coated samples in a water bath with bubbling ozone (~5% ozone) (Lee, 1989). In the process the PS is also crosslinked. The result is a mask with voids in place of

© 2003 Zikang Tang and Ping Sheng/CRC Press LLC

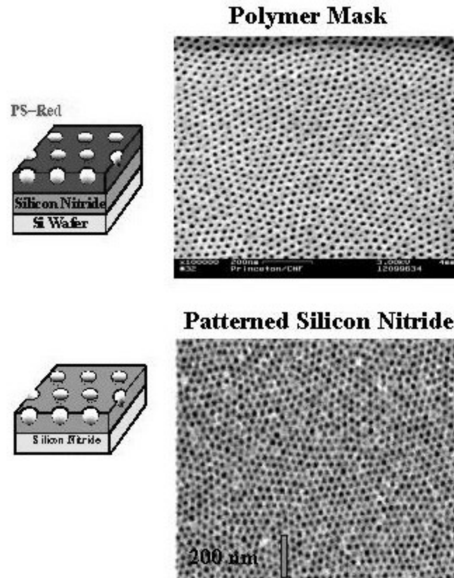

Figure 6 SEM images of mask and transferred pattern.

PB and a different thickness of PS between the air and the substrate to be patterned. As illustrated in figure 5 a CF_4 etch can now transfer the pattern into the substrate. Since the etch rates of PS and Si are comparable, the aspect ratio of the holes transferred is ~1. To make sure that polymer film is completely removed we perform an O_2 RIE as a final cleaning step. In figure 6 we show an ozonated polymer mask and the pattern transferred by RIE into SiNx. In these SEM images the contrast comes from the height profile rather than staining.

It is also possible to make a negative transfer, minority features in the diblock pattern become elevated regions on the patterned surface. In this case we use our conventional stain, OsO_4, to decorate the rubbery regions. Since CF_4 etch PB with OsO_4 at about the same rate as PS, we add a mixture CF_4/O_2 which preferentially etches PS over PB. (Cartoon in figure 5). The work in this section is largely found in Park, 1997a, Harrison, 1998c, 1998d, 1998e, 1999, 2001.

1.3.2 More Recent Developments, Multilevel, Multistep Processing

Typically different materials require slight modifications of the basic techniques outlined above. Ge reacts unfavorably with the ozonation process and therefore a thin layer of SiNx is sputtered onto its surface before the diblock layer is spun down and processed. The RIE step is then increased to eat through the SiNx and into the Ge. A cross section of a Ge Film with etched holes is shown in figure 7. Here we see the periodic pattern on the surface with N aspect ratio of the holes about 1.

© 2003 Zikang Tang and Ping Sheng/CRC Press LLC

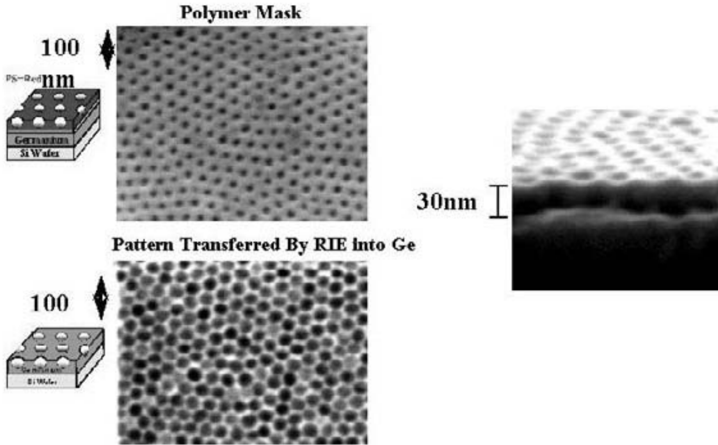

Figure 7 TEM's of mask and transferred pattern for Ge film. Note the protective layer of SiNx. Right side - cross-sectional TEM of a broken section illustrating that the aspect ratio of the etched holes is ~1.

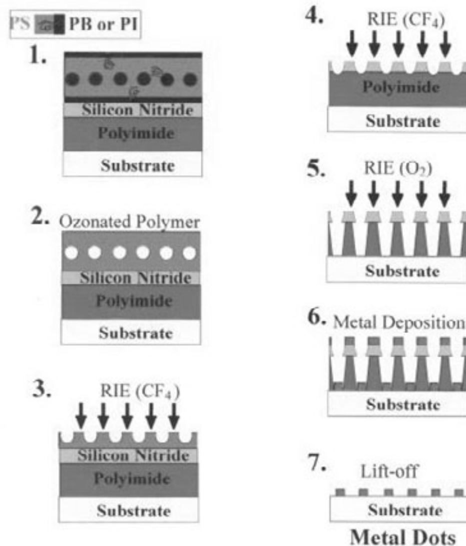

Figure 8 Trilayer technique allows a polyimide layer to planarize rough surfaces. The undercut allows easy liftoff after metal depositions.

In order to use the diblock as an evaporation mask for metal deposition we needed to enhance the aspect ratio of the mask itself and to make an undercut of the mask itself. Directly evaporating onto a polymer mask with holes through to the surface produced samples with lift off problems. The metal on the substrate surface retained contact with the metal on the mask surface. A trilayer technique solved the problem (Park, 2000). The substrate is first covered with a 50 nm layer of polyimide by spin coating

© 2003 Zikang Tang and Ping Sheng/CRC Press LLC

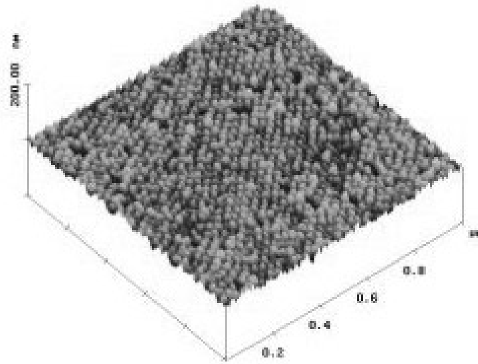

Figure 9 AFM image of Au dots prepared by trilayer technique. Lattice constant ~27 nm.

then a SiNx layer is sputtered and finally the diblock film is spun coat. The process is shown schematically in figure 8. The positive resist techniques are followed to pattern the SiNx layer and then the RIE gas is switched to O_2 which etches polyimide much more rapidly than SiNx and even leaves the desired undercut. The metal evaporation is then followed by dissolving the polyimide layer. An AFM image of Au dots produced by this technique is shown in figure 9. The trilayer technique is quite versatile since it allows the coating of most any surface. The Polyimide acts as a planarization layer to flatten rough surfaces. It therefore can be used to decorate a previously processed surface and create three dimensional structures. For example we could deposit a set of metal wires then apply the polyimide layer and SiNx etc. to evaporate a cross set of wires. In other applications we could use the large aspect ratio polyimide mask to electroplate or grow materials through the mask, figure 10, to make e.g. DNA mazes, Volkmuth, 1994.

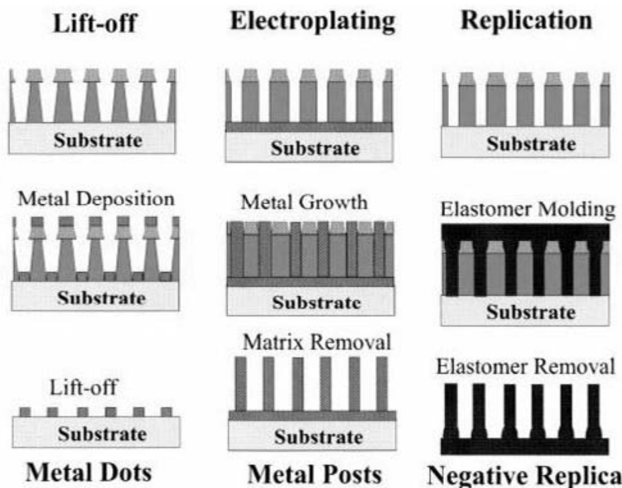

Figure 10 Other potential uses of trilayer technique.

© 2003 Zikang Tang and Ping Sheng/CRC Press LLC

Another quite successful application of the diblock lithography is in the growth of dense arrays of quantum dots (Li, 2001). In this case the compound semiconductor is covered with SiNx and the diblock. Processing progresses to the stage where there are holes in the SiNx layer. Growth of the semiconductor through the holes in the mask is accomplished by MOCVD and the mask is then removed by a wet etch. The process is schematized in figure 11 and an AFM image of GaAs quantum dots produced by this technique is shown in figure 12. Further TEM analysis of cross-section shows that the dots are epitaxial with the substrate.

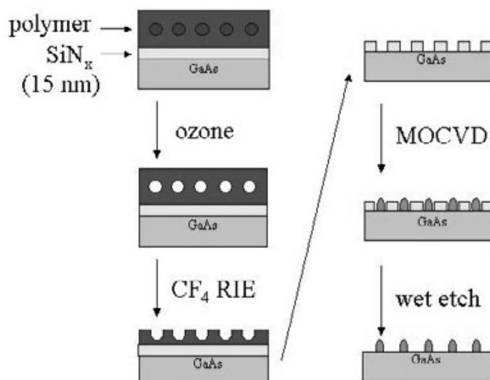

Figure 11 Processing for MOCVD selective area growth of GaAs quantum dots.

1.4 ORDERING, ANALYSIS AND CONTROL OF NANOPATTERNS

From the mask and transferred patterns it is clear that we can readily cover large areas with periodic lines and hexagonally arranged dots. However, the ordered regions are of finite extent. Perfect crystallites had a characteristic size of 20-50 periods (squared) in our early studies. For many applications, filters, quantum dots for diode lasers, etc. the size monodispersity and the density are of paramount importance. For other applications, such as conventional memory storage, we would like an addressable array with long range order covering the entire surface. (We should note that there are schemes for complete addressability do not require perfect long range order and that there are also applications such as magnetic disk recording which benefit from ordered regions on the scale of ~100 microns rather then centimeters.) Scientifically we were also interested in how perfect and long range the ordering could be made. We therefore decided to devote a considerable effort to understanding the annealing or coarsening problem and to see whether the patterns could be aligned or registered with larger scale features Harrison, 2000b, Segalman, 2001. There have been similar attempts and successes by other groups (Morkved, 1996, Kramer, 2001). The two dimensional patterns we are interested in exhibit varying degrees of both orientational and translational order. A crystalline lattice is

© 2003 Zikang Tang and Ping Sheng/CRC Press LLC

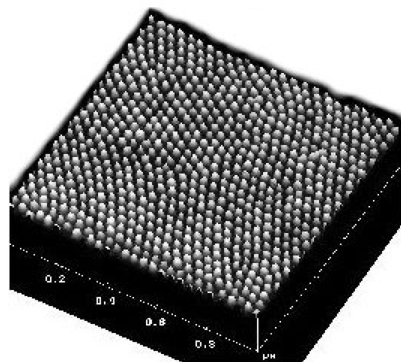

tapping-mode
atomic force
microscopy
(TMAFM)

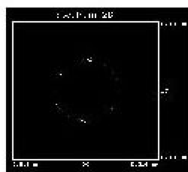

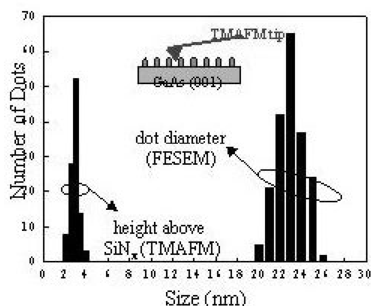

diameter:
23 ± 3 nm

overall height:
14 ± 2 nm

Figure 12 GaAs quantum dots from copolymer masks.

characterized by a set of order parameters which correspond to the amplitude and phase of density waves at all of the reciprocal lattice vectors. To consider the simplest system first we focussed on the cylindrical phase which forms the fingerprint like patterns with only two degrees of broken symmetry, one orientational and one translational (one periodicity). The symmetry of this phase is the same as for smectic liquid crystals which are layered in three dimensions or striped in two dimensions.

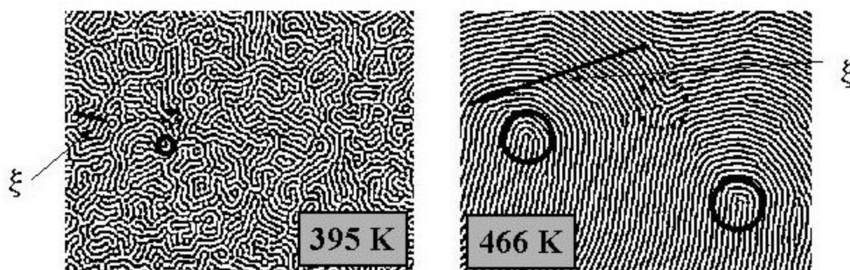

Figure 13 Cylindrical phase diblock copolymer monolayers after one hour annealing at the indicated temperatures. The size of the correlation length is indicated by the red bar. Solid circles are +1/2 disclinations and dotted circles are – 1/2 disclinations.

© 2003 Zikang Tang and Ping Sheng/CRC Press LLC

1.4.1 Correlation Functions, Fingerprints, Disclinations

In figure 13 we show two SEM images of the monolayer cylindrical phase after annealing for one hour at 395 K and 466 K. It is clear that the higher temperature anneal yields a more ordered structure. In order to make this quantitative we can define an orientation which is aligned with the stripes. As for a director field for a nematic liquid crystal the orientation is ambiguous with respect to sign or rotation by 180 degrees. It is therefore convenient to use an order parameter of the form $s(x) = s_0 e^{i2\theta(x)}$ which is the same for θ and $\theta + \pi$. Computationally the images are digitized and the orientation taken from gradients of the intensity. We can then calculate the orientational correlation function $\langle s(0)s(x)\rangle$ and fit it to a simple exponential to obtain the correlation length ξ. In figure 13 we show the time dependence of the correlation function for different annealing temperatures. Since the SEM measurement is destructive the data were taken by making a master wafer, breaking it into pieces and removing pieces successively from the annealing furnace for analysis. It is clear that higher temperatures yield longer correlation lengths and that the annealing process is quite slow at long times. The actual values of the correlation length correspond to what we observe in the images as a "grain size" or the distance at which the orientation changes by about 90 degrees. The correlation function alone does not give us a real clue as to the annealing or coarsening dynamics.

Striped patterns, like the cylindrical phase monolayers in figure 13 occur many places in nature, for us most commonly in the form of fingerprints. There is a large literature on fingerprints, mainly for identification, but there is also some work by physicists. In particular there is a paper by R. Penrose (Penrose, 1976) (which refers to the work of his father L. Penrose who did analysis of fingerprints (Penrose, 1966)) which points out the importance of the defects, loops and triradii, figure 15, which occur in fingerprints or ridged or striped phases. (Fingerprints are not completely understood, they are not genetic as evidenced by the fact that identical twins have different fingerprints.) In directed systems like nematic liquid crystals the defects are known as +1/2 and –1/2 disclinations (Kleman, 1983, Chaikin, 1995, de Gennes, 1993). For a vector field the defects are vortices with a winding number of 2π since a

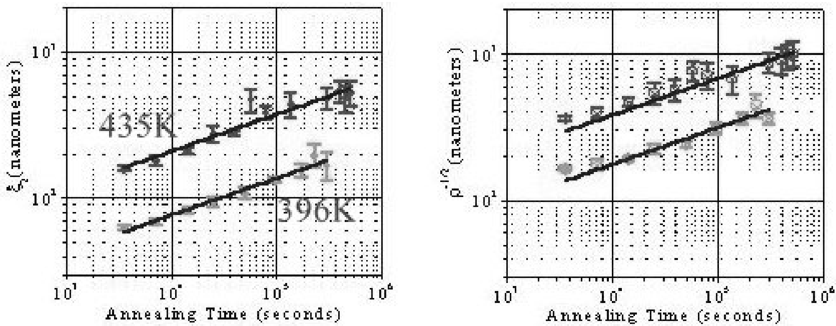

Figure 14 Correlation length and square root of inverse disclination density (separation of disclinations) for 396K and 435K annealing temperatures.

© 2003 Zikang Tang and Ping Sheng/CRC Press LLC

continuous path around a defect must rotate the vector by 2π (times an integer) to match up with the starting direction. For the rods, or stripes that make up a nematic phase the winding number can be +/- π to end up with the same orientation. Penrose pointed out that fingerprints cannot be the result of a potential or force which would act on a vector field and only allow vortex like defects. The disclinations and hence the fingerprints must be produced by a tensorial field such as a stress.

The observation that disclinations and stresses are important in striped phases is important for our studies as well. First it is clear that loops and triradii are present in our patterns (figure 13). Moreover, the density decreases as the order increases. In fact when we measured the disclination density ρ we found that it's reciprocal root $(\rho)^{-1/2}$ tracks the time and temperature dependence of the correlation length. In fact, $(\rho)^{-1/2}$, the average distance between disclinations is essentially the correlation length. This is also clear from figure 13 – compare the distance between two disclinations to the distance that it takes to "bend" the stripes by 90 degrees. What makes this interesting is that the force between disclinations is known and can be used to find the coarsening law. In the far field, several core diameters away from the disclination, and neglecting the anisotropy to find the distance dependence of the force, we can take a path around the topological defect of length $2\pi R$. Since we must accumulate an orientation change of 180 degrees over this path independent of its length, the local strain field will vary as 1/R and the strain is proportional to the stress as is the force exerted on another disclination at this distance. If we have opposite disclinations they will attract like 1/R and the response will be that they move toward one another viscously. $dR/dt \propto \mu F \propto \mu/R$, $RdR \propto dt$, $R^2 \propto t$, $R \propto t^{1/2}$ (μ is a mobility). So the distance between the disclination collapses as $R \propto t^{1/2}$. Or after time t all disclinations that were separated by R have annihilated and only ones with further separation have survived. The density of disclinations then goes down as $\rho \propto 1/R^2 \propto 1/\xi^2$ and the correlation length increases as $\xi \propto t^{1/2}$. In fact this relationship between disclination density and correlation length and the power law has been well known and experimentally tested for nematic liquid crystals. How does it work for our system? A log-log plot of disclination density and correlation length as a function of time are shown in figure 15. While the

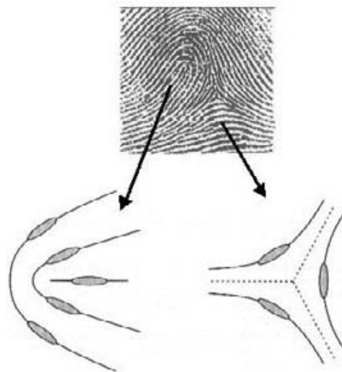

Figure 15 Top - human fingerprint with loop and triradius, corresponding to the topological defects: left) +1/2 disclination and right) –1/2 disclination.

© 2003 Zikang Tang and Ping Sheng/CRC Press LLC

correlation length indeed seems to remain the distance between disclinations ($\rho \propto \xi^{-2}$) and they obey a power law, the power law is best fit by $t^{1/4}$ rather than $t^{1/2}$.

1.4.2 Time Lapse AFM Videos and Disclination Dynamics

There have been studies of the dynamics of striped systems as well as analysis of their defect structure but usually in relation to different problems. In terms of dynamical systems fluids heated from below have been of interest for at least a century. The first instability of such a system is the formation of convective rolls carrying heat from the bottom to the top of the liquid layer. When viewed from the top the rolls form striped patterns which are dynamic and coarsen with time (at intermediate temperature differences between top and bottom, at higher differences there are further instabilities and the system goes chaotic and turbulent). This Raleigh-Benard convection problem has attracted much attention as a way of understanding pattern formation (Hou, 1997, Cross, 1995, Elder, 1992, Christensen, 1998). Along with the experiments are many theoretical treatments and especially simulations on models, such as the Swift-Hohenberg model (Cross, 1995), which hope to capture the essence of the problem. Most of the work finds that the patterns coarsen with a power law $\xi \propto t^{1/4}$ to $t^{1/5}$ depending on the magnitude of the noise term used in the simulations. These values are similar to what we have observed. But there is no general conclusion as to what is the mechanism for this coarsening. Moreover most analytical work using several different mechanisms tends to give $t^{1/2}$.

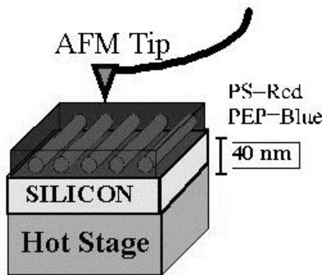

Figure 16 Cartoon of the configuration used for making time lapse AFM movies of diblock annealing. The outer blue phase is rubbery and the AFM contrast is in the elastic response.

Rather than run simulations, we decided that insight into this ¼ exponent would come only from monitoring the motion of disclinations in an experimental realization. Since our conventional imaging technique (SEM/RIE) vitrified and destroyed the sample, we were forced to develop an alternative imaging technique which was not destructive. If we invert our system so that the continuous phase is the rubber, which also preferentially wets the wafer and the air, then we can use the "tapping" mode of an AFM to sense the elastic response of the film (Hahm, 1998, figure 16. If there is a hard plastic region under the rubber surface below the tip then we will find a contrast with the region with no plastic. It is like feeling the pea under a soft pillow. The next problem is that there is no mobility at room temperature and annealing only occurs upon heating.

© 2003 Zikang Tang and Ping Sheng/CRC Press LLC

However, repeated heating in air degrades the double bond in the rubber we had been using. We therefore chemically treated the polyisoprene to saturate all of the bonds and make it polyethylpropylene (PEP) which remains rubbery but better resists degradation. We then cast the polymer on a wafer and set a piece of the wafer on a hot stage in an AFM. The movies are made by heating to 100C for one minute, cooling to room temperature taking an AFM tapping mode image, reheating, recentering the image against its small shifts, taking another image etc.

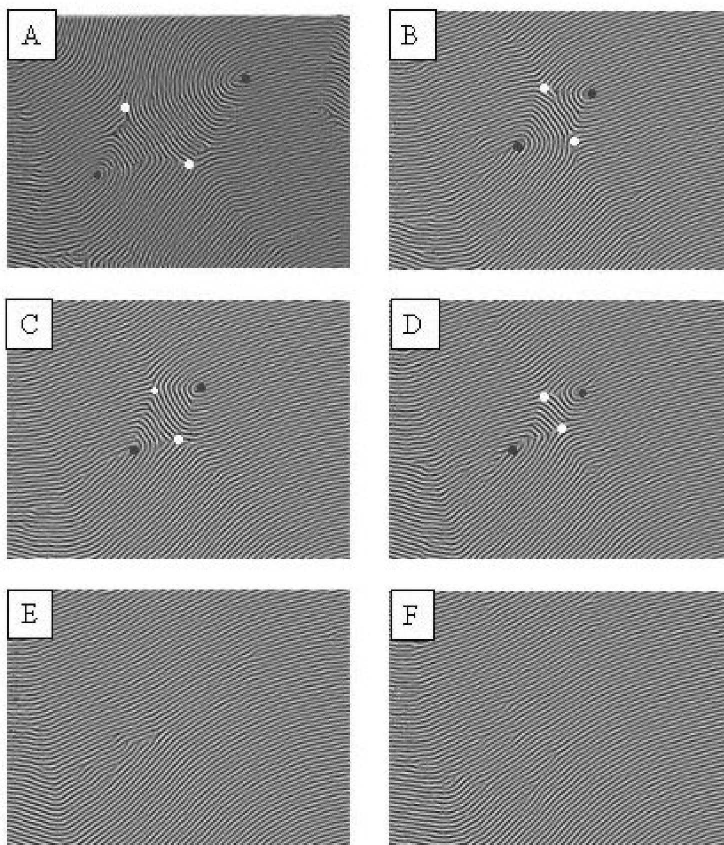

Figure 17 Quadrupole annihilation. A series of time lapse AFM images which show the most common disclination annihilation process. Sequence is across and down. We see the disclinations attract and annihilate with the creation of several dislocations which then repel. Each frame is 3 micron base.

1.4.3 Multiple Disclination Annihilation

The movies are quite spectacular and show the decrease in disclinations and the growth of the correlation length. After staring at the movies for some time, and especially on running them backward it becomes clear that the dominant process which leads to ordering is the annihilation of multiple disclinations, not just plus-

© 2003 Zikang Tang and Ping Sheng/CRC Press LLC

minus pairs. Most often it is quadrupoles, but occasionally triplets and fives, almost never two. A typical series of pictures is shown in figure 17. Here we see a characteristic $_{+}-_{-}+$ quadrupole annihilation. Once it is clear what is going on it is clear why the original dipole annihilation doesn't work. The system we are dealing with has both orientational and translational (periodic) order, it is striped or smectic, not nematic. In figure 18 we see that in order to have two disclination move toward one another, we have to break the stripes or create dislocations (Yurke, 1993, Liu, 1997), the defect associated with periodic order. In fact for every lattice step that the disclinations come together we have to introduce two dislocations. This is not energetically favorable. If, on the other hand, we can absorb the dislocation by moving other disclinations, for example in the collapse of the opposite pair in a quadrupole annihilation, then we can get rid of disclinations without creating an excess of dislocations.

We can even work out the scaling for the coarsening law. Take a characteristic length of R for the distance between all disclinations in a quadrupole. The dislocation has to move a distance R from the + disclination to the other + disclination in order for the + to move one step, dr, toward the – disclination. Since the force on the disclinations is 1/R the force on the dislocation is $1/R^2$. The dislocation has to move (viscously) a distance R at velocity $1/R^2$ which takes time $dt \propto R^3$ .The velocity of the disclination dr/dt is then proportional to $1/R^3$ which integrates to $R^4 \propto t$, $R \propto t^{1/4}$. This explains the power law that we and others studying striped phases have seen for decades. Note that it doesn't really rely on 4 disclinations, rather on the fact that we are exchanging dislocations between disclinations over a distance R.

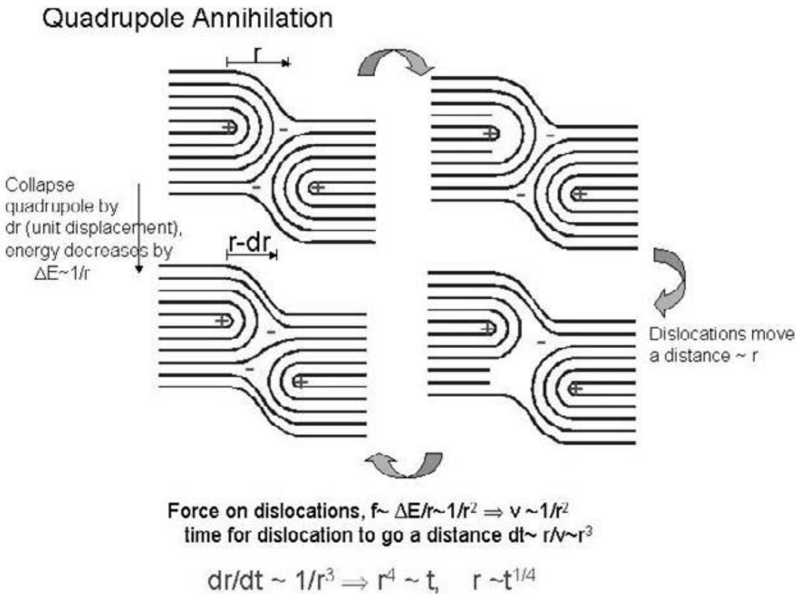

Figure 18 Cartoon of the quadrupole annihilation process, clockwise from upper left. Note in the second frame that for a disclination to advance one lattice constant requires the creation of two dislocations. To prevent the proliferation of dislocations from disclination annihilations there must be other disclinations present to absorb the dislocations.

© 2003 Zikang Tang and Ping Sheng/CRC Press LLC

Finally we should mention our annealing studies of the hexagonal phase, the two dimensional crystal. We have made time lapse movies and found that the coarsening law is similar. Unfortunately the explanation is not yet so clear. We see hardly any free disclinations. Rather the disclinations are tightly bound in dislocations and the dislocations form strings or low angle grain boundaries. However, we have not yet found a satisfactory way to define grains, largely because the strings of dislocations do not tend to form closed regions. It is more like a system of interacting strings. However, since chains of dislocations can also look like two disclinations at the chain ends, we may be getting back to the same explanation as for the stripes (or we may be going in circles).

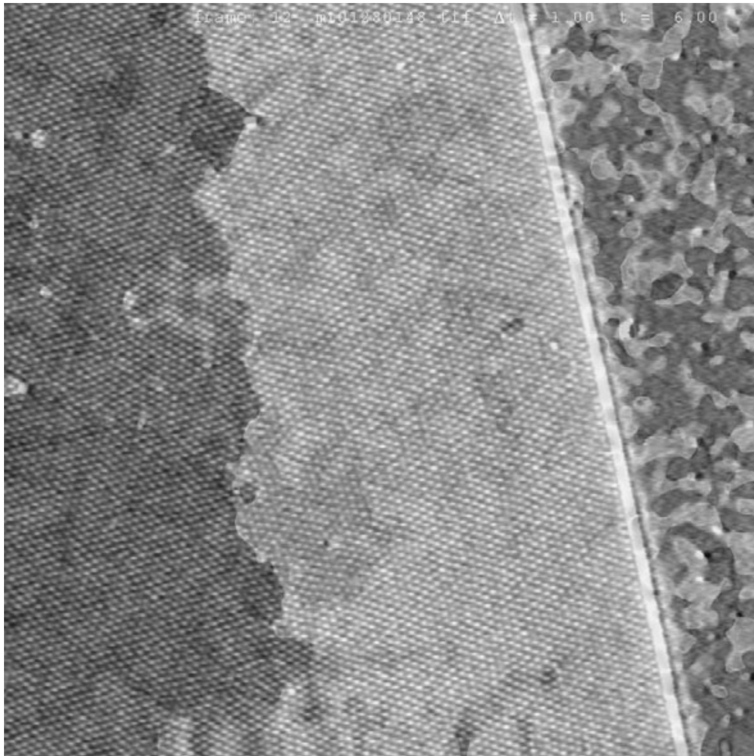

Figure 19 AFM image of Annealing of grains in a monolayer film of hexagonal spheres. There is a step edge of ~30 nm height from top to bottom on the right side. The step edge registers the first row of spheres and leads to an aligned crystallite. Further annealing leads to complete alignment of the area shown with the step edge. (Note that the area to the right of the edge is not polymer covered.)

We have also had some success at aligning the patterns. A step edge of about the same height as the monolayer nicely aligns the first row of spheres in the hexagonal phase, figure 19. Upon annealing this aligned edge serves as the growth point which completely aligns regions of several microns. More

© 2003 Zikang Tang and Ping Sheng/CRC Press LLC

spectacularly, Prof. Steve Chou's group at Princeton have shown that directly pressing on the diblock monolayer while it is heated can completely align the film over centimeter distances.

CONCLUSION

We have demonstrated that the self-assembly of diblock copolymers can serve as a useful and often unique technique for forming dense nanostructured arrays over large areas. We have extended our initial patterning to many different processes which now allow work on metal, semiconductor and insulator substrates and etching, growth and evaporation. We have also made progress in registration and alignment of the patterns so that they can we addressed. And particularly fortuitously we have found that they are very interesting systems on their own for fundamental research into the ordering and dynamics of two dimensional systems.

ACKNOWLEDGEMENT

We greatly acknowledge support from NASA and from NSF DMR9809483.

REFERENCES

Ahagon A. and Gent A. N., 1915, *J. Polym. Sci., Polym. Phys.* Ed. 13, 1285.

Anastasiadis S. H., Russell T. P., Satija S. K., Majkrzak C. F., 1989, *Phys. Rev. Lett.* 62, 1852.

Bates F. S., 1991, *Science* 251, 898.

Bates F. S. and Fredrickson G. H., 1990, *Annu. Rev. Phys. Chem.* 41, 525.

Chaikin P. M. and Lubensky T. C., 1995, *Principles of condensed matter physics*, Cambridge University Press (Cambridge, 1995).

Christensen J. J. and Bray A. J., 1998, *Phys. Rev. E* 58, 5364.

Coulon G., Ausserre D. and Russell T. P., 1990, *J. Phys. (Paris)* 51, 777.

Cross M. C. and Meiron D. I., 1995, *Phys. Rev. Lett.* 75, 2152.

de Gennes P.-G., 1979, *Scaling Concepts in Polymers* (Cornell University Press, Ithaca), p. 103.

de Gennes P. G. and Prost J., 1993, *The Physics* of *Liquid Crystals* (Oxford Science Publications, New York, ed. 2.

Elder K. R., Vinals J. and Grant M., 1992, *Phys. Rev. Lett.* 68, 3024.

Flory P. J., 1953, Principles of Polymer Chemistry (Cornell University Press, 1953), Ch. XII.

Hahm J., Lopes W. A., Jaeger H. M. and Sibener S. J., 1998, *J. Chem. Phys.* 109, 10111.

Harrison C., Park M., Chaikin P., Register R. A., Adamson D. H. and Yao N., 1998a, *Macromolecules* 31, 2185.

Harrison C., Park M., Chaikin P. M., Register R. A., Adamson D. H. and Yao N., 1998b, *Polymer* 39, 2733-2744.

© 2003 Zikang Tang and Ping Sheng/CRC Press LLC

Harrison C., Park M., Chaikin P. M., Register R. and Adamson D., 1998c, Polymeric Materials for Micro- and Nanopatterning Science and Technology (ACS Symposium Series), H. Ito, E. Reichmanis, O. Nalamasu and T. Ueno, eds. (Washington: American Chemical Society).

Harrison C., Park M., Register R. A., Adamson D. H. and Chaikin P. M., 1998d, *J. Vacuum Sci. Technol. B* 16, 544-552.

Harrison C., Park M., Chaikin P. M., Register R. A., Adamson D. H., 1998e, *Macromolecules* 31, 2185.

Harrison C., 1999, Ph.D. thesis. Princeton University.

Harrison C., Chaikin P. M., Huse D., Register R. A., Adamson D. H., Daniel A., Huang E., Mansky P., Russell T. P., Hawker C. J., Egolf D. A., Melnikov I. V. and Bodenschatz E., 2000a, *Macromolecules* 33, 857-865.

Harrison C., Adamson D. H., Cheng Z., Sebastian J. M., Sethuraman S., Huse D. A., Register R. A. and Chaikin P. M., 2000b, *Science* 290, 1558-1560.

Harrison C., Chaikin P. M. and Register R. A., 2001 Book Chapter "Block Copolymer Templates for Nanolithography", section 5.5.25 in Encyclopedia of Materials: Science and Technology, K. H. J. Buschow, R. W. Cahn, M. C. Flemings, B. Ilschner, E. J. Kramer and S. Mahajan, eds. (New York: Pergamon Press).

Hashimoto T. and Hasegawa H., 1992, *Polymer* 33, 475.

Hofstadter D., 1976, *Phys. Rev.* B 14, 2239.

Henkee C. S., Thomas E. L. and Fetters L. J., 1988, *J. Mater. Sci.* 23, 1685.

Hou Q. and Goldenfeld N., 1997, *Physica* A 239, 219.

Huang E., Russell T. P., Harrison C., Chaikin P. M., Register R. A., Hawker C. J. and Mays J., 1998, *Macromolecules* 31, 7641-7650.

Huang E., Mansky P., Russell T. P., Harrison C., Chaikin P. M., Register R. A., Hawker C. J. and Mays J., 2000, *Macromolecules* 33, 80-88.

Jones R. A. L., Norton L. J., Shull K. R., Kramer E. J., Felcher G. P., Karim A. and Fetters L. J., 1992, *Macromolecules* 25, 2539.

Kleman M., 1983, *Points, Lines and Walls* (Wiley, New York, 1983).

Lee J. S., Hirao A. and Nakahama S., 1989, *Macromolecules* 22, 2602.

Leibler L., 1980, *Macromolecules* 13, 1602.

Li R. R., Dapkus P. D., Thompson M. E., Jeong W. G., Harrison C., Chaikin P. M., Register R. A. and Adamson D. H., 2000, *Appl. Phys. Lett.* 76: 13, 1689-1691.

Liu C. and Muthukumar M., 1997, *J. Chem. Phys.* 106, 7822.

Mansky P. and Russell, T. P., 1995, *Macromolecules* 28, 8092.

Mansky P., Chaikin P. M. and Thomas E. L., 1995, *J. Mat. Sci.* 30, 1987.

Mansky P., Harrison C. K., Chaikin P. M., Register R. A. and Yao N., 1996, *Appl. Phys. Lett.* 68, 2586.

Morkved L., Wiltzius P., Jaeger H. M., Grier D. G. and Witten T. A., 1994, *Appl. Phys. Lett.* 64, 422.

Morkved L., Lu M., Urbas A. M., Ehrichs E. E., Jaeger H. M., Mansky P. and Russell T. P., 1996, *Science* 273, 931.

Morton M. and Fetters L. J., 1975, *Rubber Chem. Technol* 48, 359.

© 2003 Zikang Tang and Ping Sheng/CRC Press LLC

Park M., Chaikin P. M., Register R. A. and Adamson D. H., 2001, *Appl. Phys. Lett.* 79, 257-259.
Park Miri, Harrison C., Chaikin P. M., Register R. A. and Adamson D. H., 1997a, *Science* 276, 1401.
Park M., Harrison C., Chaikin P. M., Register R. A., Adamson D. H. and Yao N., 1997, Volume 461: *Morphological Control in Multiphase Polymer Mixtures*, Materials Research Society, Boston, MA, Dec 2-6, 1996; Materials Research Society: Pittsburgh, PA, 1997b; pp. 179-184.
Penrose L. S., 1965, *Nature*.
Penrose R., 1979, *Ann. Hum. Genet*, London, 42, 435.
Radzilowski L. H. and Thomas, E. L., 1996, *J. Polym. Sci. B: Polym. Phys.* 34, 3081.
Segalman R. A., Yokoyama H. and Kramer E. J., 2001, *Adv. Mater.* 13, 1152.
Thouless D. J., Kohmoto M., Nightingale M. P. and den Nijs M., 1982, *Phys. Rev. Lett.* 49, 405.
Volkmuth W. D., Duke T., Wu M. C., Austin R. H. and Szabo A., 1994, *Phys. Rev. Lett.* 72, 2117.
Yurke B., Pargellis A. N., Kovacs T. and Huse D. A., 1993, *Phys. Rev. E* 47, 1525.

© 2003 Zikang Tang and Ping Sheng/CRC Press LLC